THE THERMODYNAMICS OF URANOPHANE DISSOLUTION AND GROWTH IN $CACL_2$-SIO_2(AQ) TEST SOLUTIONS

James D. Prikryl

Center for Nuclear Waste Regulatory Analyses

Southwest Research Institute®, 6220 Culebra Rd., San Antonio, Texas 78238, USA

Abstract

The thermodynamics of dissolution and growth of uranophane [$Ca(UO_2)_2(SiO_3OH)_2 \cdot 5H_2O$] have been examined in Ca- and Si-rich test solutions at low temperatures {20.5 ± 2.0 °C [68.9 ± 3.6 °F]} and near-neutral pH (~6.0). Uranophane is the end phase of the paragenetic sequence of uranyl minerals that are produced by corrosion of spent nuclear fuel and weathering of uraninite in U ore deposits hosted by siliceous volcanic rocks. Due to its long-term chemical stability and potential to incorporate spent fuel waste species, uranophane will influence the long-term dissolved concentration and mobility of radionuclides at the potential nuclear waste geologic repository at Yucca Mountain, Nevada. Batch-type experiments were designed to approach uranophane equilibrium from both undersaturation and supersaturation. Experimental solutions were prepared in matrices of ~10^{-2} M $CaCl_2$ and ~10^{-3} M or ~2×10^{-3} M SiO_2(aq). Test solutions undersaturated with uranophane had initial U concentrations of 0.0 or ~10^{-7} M. Test solutions supersaturated with uranophane had initial U concentrations of ~10^{-6} M or ~2×10^{-6} M. The test solutions were reacted with synthetic uranophane (confirmed by X-ray diffraction and chemical analyses) and analyzed periodically over 10 weeks. Interpretation of the aqueous solution data permitted extraction of an equilibrium constant for the uranophane dissolution reaction (log K = 11.18 ± 0.54) and standard state Gibbs free energy of formation for uranophane {ΔG°_f = -6,195.2 ± 3.1 kJ mol^{-1} [-1.4807×10^6 ± 740.9 cal mol^{-1}]}.

1. INTRODUCTION

Yucca Mountain, Nevada, is being evaluated as a potential geologic repository site for disposal of high-level nuclear waste (HLW). Most of the HLW to be housed at Yucca Mountain is spent nuclear fuel (SNF) derived from nuclear reactors. SNF is 95% UO_2 with the remainder composed of highly radioactive fission and activation products and actinides (Oversby, 1994; Johnson and Shoesmith, 1988). Previous studies have shown that under the moist, oxidizing conditions expected at the potential Yucca Mountain repository, SNF is thermodynamically unstable (Finch and Ewing, 1992; Finch et al., 1999; Finn et al., 1998; Wronkiewicz et al., 1992, 1996). If SNF is exposed to water in a potential Yucca Mountain repository, it will likely undergo dissolution, leading to the formation of secondary uranyl (U^{6+}) phases that may persist for thousands of years (Finch et al., 1996). Crystallographic theory indicates that low solubility radionuclides of SNF (e.g., Np and Pu) may be incorporated in the structures of relatively stable secondary uranyl phases (Burns et al., 1997). The solubility of secondary uranyl phases may therefore influence the long-term dissolved concentration and mobility of low solubility radionuclides of SNF at a potential Yucca Mountain repository.

The general sequence of secondary uranyl minerals formed during oxidative alteration of SNF and weathering of naturally occurring uraninite (UO_{2+x}, an analog to UO_2 in SNF) in silica-rich systems consists initially of uranyl oxide hydrates followed by uranyl silicates (Finch and Murakami, 1999; Finch et al., 1999; Pearcy et al., 1994; Wronkiewicz et al., 1992, 1996). Long-term leaching studies of unirradiated UO_2 and SNF designed to simulate conditions at a potential Yucca Mountain repository indicate that the calcium uranyl silicate uranophane [$Ca(UO_2)_2(SiO_3OH)_2 \cdot 5H_2O$], along with the alkali uranyl silicates boltwoodite [$KH(UO_2)SiO_4 \cdot 1.5H_2O$] and Na-boltwoodite [$(Na,K)H(UO_2)SiO_4 \cdot 1.5H_2O$], are the dominant end products of spent fuel alteration

(Finch et al., 1999; Wronkiewicz et al., 1992, 1996). Uranophane is also the dominant end product of the oxidative weathering of uraninite hosted in silicic volcanic rocks at the Nopal I U deposit in Chihuahua, Mexico—a natural analog to the potential HLW repository at Yucca Mountain (Pearcy et al., 1994).

Recent experimental data on the synthesis of uranyl compounds from solutions containing Np^{5+} indicate that Np may be incorporated in uranophane (Burns et al., 2004; Douglas et al., 2005). Neptunium-237 is present in SNF at 400–600 ppm and, due to its long half-life (2.14×10^6 years) and potentially high mobility in chemically oxidizing groundwater, may be one of the most important radionuclides for long-term performance of a potential Yucca Mountain repository. Dating of uranophane from the Nopal I U deposit has yielded a radiometric determined age (U-Pb isochron method) of 3.2 to 3.4 Ma [3.2×10^6 to 3.4×10^6 years] (Pickett and Murphy, 1997). U-series disequilibrium measured on a single uranophane from the Nopal I U deposit yielded an age of 320 ± 30 ka [320,000 ± 30 years] (Pickett and Leslie, 2005). Due to the long-term chemical stability of uranophane and its potential to incorporate Np, uranophane may have a significant influence on the long-term performance (i.e., 10^4 to 10^6 years) of the potential repository at Yucca Mountain. For example, Np incorporation in uranophane may control the concentration of Np in solution during SNF degradation, which is risk significant in dose calculations at the potential Yucca Mountain repository.

Despite the potential significance of uranophane at Yucca Mountain, the thermodynamic parameters required for predictive modeling and interpretations of chemical interactions among uranophane and groundwater are poorly known. In this study, the thermodynamics of uranophane dissolution and growth were investigated by reacting uranophane in chemically oxidizing, Ca- and Si-rich solutions predicted to bracket uranophane solubility. Based on preliminary data on uranophane dissolution from this study, Prikryl and Murphy (2004) reported provisional thermodynamic data for

uranophane dissolution (i.e., log Qs ranging from 10.54 to 11.06). In this report, the data on uranophane dissolution reported by Prikryl and Murphy (2004) are supplemented with additional data on uranophane dissolution and evaluated together with data on uranophane growth. Because natural uranophane samples are typically of insufficient quantity and purity for use in thermodynamic experiments, the experiments were performed using synthesized uranophane. Evaluation of aqueous solution chemistry data from the uranophane solubility experiments permits extraction of an equilibrium constant and standard state Gibbs free energy of formation for uranophane.

2. EXPERIMENTAL MATERIALS AND METHODS

2.1. Uranophane Synthesis

Uranophane was synthesized based on the method of Vochten et al. (1997). The method entails initial synthesis of boltwoodite followed by conversion to uranophane by exchange of Ca^{2+} for K^{+} in the crystalline structure of the uranyl silicate.

To synthesize boltwoodite, 9.28 g [0.327 oz] of uranyl nitrate hexahydrate [$UO_2(NO_3)_2 \cdot 6H_2O$] and 1.33 g [0.047 oz] of KCl were dissolved in 200 mL [6.76 fl oz] of deionized (DI) water. The resultant solution was adjusted with 1 M KOH to a pH of 11.5. The solution was transferred into the teflon liner of a 2-L [67.6 fl oz] Parr pressure reactor (Parr Model 4522, Parr Instruments, Moline, IL). Approximately 32 g [1.13 oz] of ultrasonically cleaned natural rock crystal quartz fragments (Wards Geology, Rochester, NY) were added to the mixture in the teflon liner. The quartz fragments had widths or diameters >0.5 cm [>0.2 in] (prepared by breaking pieces of rock crystal quartz in an agate mortar and pestle). The reaction vessel was heated to 185 °C [365 °F], and the contents were allowed to react for 4 days.

After cooling to room temperature, the resultant mixture was filtered through a Spectra/Mesh® fluorocarbon filter (Spectrum, Houston, TX) having 210-µm [8.27×10^{-3} in] mesh openings to remove the quartz fragments. The resultant solid consisted of pale yellow acicular crystals and a white-colored, gel-like precipitate. This precipitate was separated from the yellow crystals by washing with 5% acetic acid, centrifugation, and supernatant decantation. This process was repeated three times to adequately dissolve and remove the gel-like precipitate. The mixture was then vacuum-filtered and washed several times with DI water to remove the acetic acid. The remaining solid consisted of fine, pale-yellow needles of boltwoodite [confirmed by chemical analysis and X-ray diffraction (XRD)].

To obtain uranophane, approximately 1-g [0.035 oz] fractions of the synthesized boltwoodite were placed in 100-ml [3.38-fl oz] teflon vessels with 50 ml [1.69 fl oz] of 2 M $CaCl_2$. The vessels were sealed and placed in a 125 °C [257 °F] oven for 15 days. Every 3 days during the 15-day period, the vessels were removed, the supernatant was decanted, and a new 50-ml [1.69-fl oz] aliquot of 2 M $CaCl_2$ was added to the vessels. After 15 days, the resultant mixtures were vacuum-filtered and washed several times with DI water. The remaining solids consisted of fine {generally <50 µm [<1.97×10^{-3} in] in length} yellow acicular crystals (Fig. 1A).

XRD confirmed the acicular crystals to be uranophane. An XRD pattern for the synthetic uranophane is shown in Fig. 1B, together with a reference pattern for natural uranophane taken from the International Centre for Diffraction Data (ICDD) database (1993). The synthetic uranophane XRD pattern was obtained using an automated (RADIX) Siemans D–500 X-ray diffractometer (CuKα radiation, Ni filter, 40 kV, 37 mA; scan 5°–40° 2-theta at 0.02° step; count time 1.0 s). Correspondence between the sample and reference patterns is good. Two small peaks (at 26.9° and 28.2° 2-Theta) appear in the pattern for the synthesized sample, but are absent in the reference pattern.

However, these peaks are reported in a reference pattern for natural uranophane (Powder Diffraction File Number 8-442) from the ICDD Minerals Data Book (1986) and appear in uranophane synthesized by Nguyen et al. (1992). The magnitude and sharpness of the peaks in the XRD pattern indicate that the synthesized uranophane is well crystallized.

Chemical analyses of the synthesized uranophane were performed using a whole rock procedure that entails complete dissolution of the sample in 0.1 M HCl followed by inductively coupled plasma spectrometry (ICP) for major cations (e.g., Ca, K, and Si) and ICP mass spectrometry (ICP-MS) for uranium. Using measured analytical contents, stoichiometric coefficients for Ca:Si:U in the synthesized uranophane were calculated to be 0.99 (±0.01):1.99(±0.01):1.99(±0.07), which corresponds to values expected for ideal uranophane (1:2:2, respectively). Chemical analyses indicated K contents of 1.5–2.1 ppm in the synthesized uranophane, suggesting that some residual boltwoodite may be present. However, XRD analyses did not detect the presence of boltwoodite in the synthesized solids, indicating little or no residual boltwoodite. The K contents could be due to the presence of other impurities (e.g., incomplete removal of the gel-like material precipitated with boltwoodite during the synthesis process).

2.2. Dissolution and Precipitation Experiments

Uranophane solubility experiments were designed to approach uranophane equilibrium from both undersaturation and supersaturation in Ca- and Si-rich solutions. Experimental solutions were prepared in matrices of ~10^{-2} M $CaCl_2$ and ~10^{-3} or ~2×10^{-3} M SiO_2(aq). Test solutions for uranophane dissolution (i.e., solutions undersaturated with uranophane) were prepared to have initial U concentrations of 0.0 and ~10^{-7} M. The initial concentrations of U in experimental solutions for uranophane precipitation

(i.e., solutions supersaturated with uranophane) were determined from the results of the uranophane dissolution experiments (reported hereinafter). These results indicated that experimental solutions were in near- equilibrium with uranophane in the latter stages of the dissolution experiments (i.e., after test solutions had reacted with uranophane for 6 weeks). Based on these late stage solution compositions, experimental solution compositions estimated to be supersaturated with uranophane were prepared to have initial U concentrations of ~10^{-6} and ~2×10^{-6} M.

Before addition of uranophane, the pHs of the dissolution and precipitation test solutions were adjusted to ~6.0 by addition of $CaCO_3$ and allowed to equilibrate with atmospheric CO_2(g) for 2 weeks. The solubility experiments were carried out by reacting measured amounts of these solutions {200.0 ± 0.3 g [7.05 ± 0.01 oz]} with measured amounts of synthetic uranophane {0.500 ± 0.001 g [0.01764 ± 0.00003 oz]} in 250-ml [8.45-fl oz] polypropylene bottles. Experiments were conducted at room temperature {20.5 ± 2.0 °C [68.9 ± 3.6 °F]} under atmospheric PCO_2 conditions. Solutions were continuously agitated during the experiments using a gyratory shaker.

For the dissolution experiments, two 5-ml [0.17-fl oz] aliquots of the experimental solutions were taken at 24 hours and then at 1-week intervals for 10 weeks. For the precipitation experiments, two 5-ml [0.17-fl oz] aliquots of the experimental solutions were taken at 24 and 48 hours and then at 1-week intervals for 10 weeks. Before each sampling, the test solutions were centrifuged to remove suspended solids. Test solution weights were measured before and after sampling to track loss of solution due to sampling and evaporation. The pH of one of the 5-ml [0.17-fl oz] aliquots was measured immediately after sampling using a ROSS™ semi-micro glass combination pH electrode (Thermo Orion, Beverly, MA). The other 5-ml [0.17-fl oz] aliquot was acidified to pH <2.0 by addition of concentrated HNO_3. Concentrations of cations in the acidified aliquots were determined by ICP-AES; U concentrations were measured by ICP/MS.

3. RESULTS

3.1. Experimental Data

The initial pH and concentrations of Ca, Si, and U measured in the test solutions for the uranophane solubility experiments are listed in Table 1. Dissolution test solutions (i.e., solutions undersaturated with uranophane) are labeled D–0A, D–0B, D–7A, and D–7B in Table 1, and precipitation test solutions (i.e., solutions estimated to be supersaturated with uranophane) are labeled P–1A, P–1B, P–2A, and P–2B. Measured initial pHs and concentrations of Ca, Si, and U in the dissolution and precipitation test solutions were at or near their intended values (see Table 1).

3.1.1. Dissolution experiments

The pHs and concentrations of Ca, Si, and U measured in the dissolution test solutions as a function of reaction time are plotted in Fig. 2. The values plotted at time 0 represent solutions prior to addition of uranophane.

Plots of solution pH show relatively constant pH over the first week of the tests and then a general decrease in pH from week 2 to week 5 (Fig. 2). Over the remainder of the tests (i.e., from week 6 to week 10), the pH of the dissolution test solutions remained relatively constant, ranging from 5.86 to 5.92. Small up and down variations in solution pH over the duration of the tests suggest some systematic analytical errors.

An initial increase in the U content of the uranophane dissolution test solutions is observed at the 24-hour sampling interval (Fig. 2). From 24 hours to week 2, U contents tended to increase slightly in the tests solutions. With the exception of several outliers (e.g., weeks 4 and 10 of test D–0A, weeks 4 and 7 of test D–0B, weeks 5 and 7 of test D–7A, and weeks 6 and 10 of test D–7B), U contents over the remainder of the tests (i.e., from week 3 to week 10) varied over a relatively narrow concentration range

(i.e., 1.84×10^{-7} to 3.06×10^{-7} M). From 24 hours to week 3, Ca contents in test solutions were generally unstable. With the exception of the week 10 sampling interval of test D–7B, a generally smooth trend of increasing Ca content in the test solutions was observed from week 4 onward. Si contents in the test solutions were observed to generally decrease over the first 3 or 4 weeks of the tests and then to generally increase over the remainder of the tests (i.e., from week 5 to week 10). Up and down variations in U, Ca, and Si contents of each test solution over the duration of the dissolution tests are attributed to analytical and sampling errors.

3.1.2. Precipitation experiments

The pHs and concentrations of Ca, Si, and U measured in the precipitation test solutions as a function of reaction time are plotted in Fig. 3. The values plotted at time 0 represent solutions prior to addition of uranophane.

With the exception of test solution P–1A, a trend of decreasing solution pH was observed over the first 2 weeks of the tests (Fig. 3). Over the remainder of the tests (i.e., from week 3 to week 10, excluding test P–1A), the pH of test solutions remained relatively constant, ranging from 5.78 to 5.84. In test solution P–1A, solution pH increased over the first 24 hours of the test and then decreased over the first week of the test. From week 1 to week 4 of test P–1A, a trend of increasing solution pH was observed; over the remainder of the test, solution pH remained relatively constant, ranging from 5.94 to 5.95. Systematic analytical errors are again suggested by small up and down variations in solution pH over the duration of the tests.

An initial decrease in U, Ca, and Si contents in the precipitation test solutions is observed at the 24-hour sampling interval (Fig. 3). In general, from 24 to 48 hours, U, Ca, and Si contents in the test solutions remained relatively constant. With the exception of a few outliers (e.g., weeks 8 and 10 of test P–1A, week 9 of test P–1B,

week 8 of test P–2A, and week 7 to test P–2B), U contents generally increased over the remainder of the tests (i.e., from week 1 to week 10). From the 48-hour sampling interval onward, a general trend of increasing Ca content in the test solutions was also observed. Like U, the Ca data contained some outliers (e.g., weeks 1, 5, and 9 of test P–1A, week 6 of test P–1B, and weeks 1 and 9 of test P–2B). Si contents in the test solutions tended to decrease over the first 2 weeks of the tests and then remained relatively constant over the remainder of the tests. As in the dissolution tests, up and down variations in U, Ca, and Si contents of each test solution over the duration of the precipitation tests are attributed to analytical and sampling errors.

3.2 Mass Transfer Relations

Thermodynamic and kinetic interpretation of the uranophane solubility data requires knowledge of mass transfer (i.e., moles of Ca, Si, and U released or precipitated) as a function of time and solution chemistry. The cumulative release in a dissolution or precipitation experiment is given by

$$n_{I,R}(t_s) = m_I(t_s)W(t_s) + n_{I,E}(t_s) - m_I(t_0)W(t_0) \quad (1)$$

where $n_{I,R}(t_s)$ is the net number of moles of a component I (e.g., Ca, Si, or U) released to solution at the time of sampling (t_s) (which is negative for net precipitation), $m_I(t_s)$ is the molality of I in the solution at time t_s, $m_I(t_0)$ is the molality of I in solution at the start of the experiment (t_0), $W(t_s)$ is the mass of solution prior to sampling at t_s, $W(t_0)$ is the mass of solution at time t_0, and $n_{I,E}(t_s)$ is the number of moles of I extracted in all solution samples

removed at all times t_p prior to time t_s, which is given by

$$n_{I,E}(t_s) = \Sigma\, m_I(t_p) W_E(t_p) \qquad (2)$$

where $m_I(t_p)$ is the molality of I in solution taken at time t_p, and $W_E(t_p)$ is the mass of solution extracted in the sample taken at time t_p. Measurements of experimental solution masses before and after sampling provide values of W and W_E, which allow effects of variations in solution mass due to sampling and evaporation to be explicitly accounted for in the cumulative mass transfer calculations.

Because of the variable solution mass, cumulative moles released corresponding to each sampling time and analytical measurement depend on measured concentrations for all earlier experimental times. Spurious analytical data will therefore adversely influence calculated values of the total mass released for all subsequent times. To minimize the effect of the spurious analytical concentrations of Ca and U noted in Section 3.1.1 for the dissolution experiments and in Section 3.1.2 for the precipitation experiments, interpolated Ca and U concentrations were used to calculate solute masses extracted at these sampling times. The interpolated concentrations were also used in calculation of cumulative moles of Ca and U released at each sampling time.

3.2.1. Dissolution experiments

Results of the mass transfer calculations for Ca, Si, and U (i.e., moles of Ca, Si, and U released or precipitated as a function of time and solution chemistry) in the uranophane dissolution tests are illustrated in Fig. 4. The mass transfer data indicate net release of Ca and U and net precipitation of Si over the duration of the tests.

Over the first 24 hours of the dissolution tests, mass transfer of Ca and U was characterized by release and, with the exception of test D–7B, mass transfer of Si was

characterized by precipitation. After the initial effects, mass transfer in the first half of the dissolution tests (i.e., from 24 hours to week 4 or 5) was generally characterized by erratic Ca release, continued Si precipitation, and, with the exception of test D–7A, continued U release. After initial U release, test D–7A was characterized by slight precipitation of U from week 2 to week 4 of the dissolution tests.

Over the second half of the dissolution tests (e.g., from 5 or 6 weeks onward), mass transfer was generally characterized by up and down deviations in Ca, Si, and U release. However, the moles of Ca, Si, and U released in each of the test solutions varied over a relatively narrow range. Explanations for the up and down variations in Ca, Si, and U release in the second half of the tests include carryover of analytical errors in the Ca, Si, and U concentration data to the mass transfer calculations and/or the possible occurrence of suspended solids (e.g., uranophane colloids) in the sampled test solutions.

3.2.2. Precipitation experiments

Results of the mass transfer calculations for Ca, Si, and U in the uranophane precipitation experiments are illustrated in Fig. 5. The mass transfer data indicate net precipitation of Ca, Si, and U over the duration of the experiments.

Mass transfer of Ca, Si, and U over the first 24 hours of the precipitation tests was characterized by precipitation. After 24 hours, mass transfer in the early part of the precipitation tests (i.e., from 24 hours to 4 weeks) was generally characterized by erratic release of Ca, continued Si precipitation, and steady release of U.

Over the second half of the precipitation tests (e.g., from week 5 onward), mass transfer of Ca, Si, and U was characterized by up and down variations in release. However, like release in the dissolution experiments, the moles of Ca, Si, and U released in each test solution varied over a relatively narrow range. Again, explanations

for the up and down variations in Ca, Si, and U release include the carryover of analytical errors in the Ca, Si, and U concentration data to the mass transfer calculations and/or the possible occurrence of suspended solids in the sampled test solutions.

3.3. Thermodynamic Calculations

The equilibrium reaction for uranophane dissolution can be written as

$$Ca(UO_2)_2(SiO_3OH)_2 \cdot 5H_2O + 6H^+ \leftrightarrow Ca^{2+} + 2UO_2^{2+} + 2SiO_2(aq) + 9H_2O. \quad (3)$$

The corresponding reaction quotient for uranophane is defined by

$$Q = [Ca^{2+}]\,[UO_2^{2+}]^2\,[SiO_2(aq)]^2\,[H^+]^{-6} \quad (4)$$

where the square brackets represent thermodynamic activities corresponding to a standard state of a one molal solution referenced to infinite dilution. Using the pH and concentrations of Ca, Si, and U measured in the dissolution and precipitation test solutions and assuming equilibrium with atmospheric PCO_2, activities of the aqueous species in Eq. 4 were determined using the EQ3NR Version 7.2b geochemical code with the Data0.com.R2 database (Wolery, 1992). Reaction quotients for the experimental solutions were then calculated using Eq. 4.

The range in the logarithms of activities of Ca^{2+}, $SiO_2(aq)$, UO_2^{2+}, and H^+ and the range in the calculated logarithms of the reaction quotient (log Q) for uranophane dissolution in each of the dissolution and precipitation test solutions are listed in Table 2. Log Qs for uranophane dissolution obtained from test solution chemistries as a function of time are plotted in Fig. 6.

The activities of Ca^{2+} and SiO_2(aq) in each test solution over the duration of the experiments were relatively constant compared to the activities of UO_2^{2+} and H^+ (Table 2). The activities of Ca^{2+} and SiO_2(aq) varied by 0.02 to 0.03 log units in the dissolution tests and by 0.01 log units in the precipitation tests. Over the duration of the dissolution tests, the activities of UO_2^{2+} varied from 0.28 log units (test D–7A) to 0.58 log units (test D–0A), and H^+ activities varied from 0.15 log units (test D–0A) to 0.18 log units (tests D–7A and D–7B). Over the duration of the precipitation tests, UO_2^{2+} activities varied from 0.88 log units (test P–1A) to 1.11 log units (test P–2A), and H^+ activities varied from 0.15 log units (test P–1B) to 0.17 log units (test P–2A).

Log Qs over the duration of the dissolution tests ranged from 10.54 to 11.18 and over the duration of the precipitation tests from 10.20 to 12.22 (Table 2; Fig. 6). Because the activities of Ca^{2+} and SiO_2(aq) in each test solution were relatively constant, they had little influence on variations in log Q values. Variations in log Qs were influenced primarily by changes in solution pH (i.e., $[H^+]$) and the activity of UO_2^{2+}. The wider range in log Q values in the precipitation experiments (10.20 to 12.22) compared to the dissolution experiments (10.54 to 11.18) was the result of differences in the SiO_2(aq) activities of the test solutions. In the precipitation tests, Si concentrations of test solutions P–2A and P–2B were approximately two times greater than test solutions P–1A and P–2A (see Table 1). Aqueous speciation of measured test solution chemistries using the EQ3NR Version 7.2b geochemical code indicated that the higher range of log Qs in tests P–2A and P–2B (10.90 to 12.22) compared to the range of log Qs in tests P–1A and P–1B (10.20 to 11.48) was the result of higher SiO_2(aq) activities rather than differences in pH or UO_2^{2+} activities.

4. DISCUSSION

The dissolution and precipitation experiments were designed to bracket the uranophane solubility limit. Initial chemical conditions were selected so that reaction of uranophane with experimental solutions would approach equilibrium from both undersaturation and supersaturation. Sampling schemes were chosen to track the mass transfer of uranophane components (i.e., moles of Ca, Si, and U) as a function of time and solution chemistry. Possible complications in the mass transfer of uranophane components were limited by measuring experimental solution masses before and after sampling, which allowed variations in solution mass due to sampling and evaporation to be explicitly accounted for in cumulative mass transfer calculations. In addition, to reduce the effect of spurious analytical concentrations on cumulative mass transfer of Ca and U, interpolated Ca and U concentrations were used in mass transfer calculations at sampling times noted in Section 3.1.1 for the dissolution tests and in Section 3.1.2 for the precipitation tests. Mass transfer results reveal characteristics of the reaction paths that permit evaluation of uranophane equilibrium and calculation of uranophane thermodynamic properties.

4.1 Solution Chemistry and Reaction Path Characteristics

Disregarding spurious Ca and U analytical concentrations (see Sections 3.1.1 and 3.1.2), solution chemistries in both the dissolution and precipitation tests were generally characterized by small up and down variations along generally smooth trends in pH and Ca, Si, and U concentrations as a function of time (Figs. 2 and 3). The up and down variations in pH and in Ca, Si, and U concentrations were likely due to a combination of analytical and sampling errors. The ROSS™ semi-micro glass combination pH electrode used to measure pH had an uncertainty of ± 0.03 pH units. Based on comparison of expected and measured values of calibration standards, measurement of

Ca and Si by ICP had uncertainties of ± 6% and ± 5%, respectively. Likewise, measurement of U by ICP/MS had an uncertainty of ± 3%. Measurement uncertainties could account for most, if not all, of the up and down variations along general trends in pH and in Ca and Si concentrations.

Uranium analyses included a number of measurements which exceeded variations in U that might be expected to result from analytical uncertainty. For example, precipitation test solutions included several relatively high U measurements, interrupting generally smooth trends in the data (e.g., weeks 5, 6, and 10 of test P–1B; weeks 4 and 10 of test P–2A; and weeks 2 and 6 of test P–2B). Although test solutions were centrifuged prior to sampling to remove suspended solids, the relatively high U contents suggest that uranophane colloids may have been present in the sampled experimental solutions. However, analyses using interpolated U concentrations in place of the relatively high U contents did not have a significant effect on cumulative mass transfer of U. Therefore, measured U concentrations were used in subsequent calculations for determination of an equilibrium constant for uranophane.

The up and down variations in Ca, Si, and U concentrations are reflected as up and down variations in the mass transfer data as a function of time. However, like the concentration data, these variations do not mask general trends in the mass transfer data. General trends and characteristics in pH and in Ca, Si, and U concentrations and mass transfer are summarized below.

4.1.1. pH

Reaction of synthesized uranophane with the dissolution test solutions was characterized by relatively constant pH over the first week of the tests and then a general decrease in pH up to week 5 (Fig. 2). Over the latter stages of the tests (i.e.,

from week 6 to 10), solution pH in the dissolution tests remained relatively constant (pH range of 5.86–5.92).

With the exception of test solution P-1A, reaction of synthesized uranophane with the precipitation test solutions was characterized by relatively constant pH over the first 24 hours of reaction, a general decrease in pH up to week 2 of the tests, and then relatively constant pH over the remainder of the tests (Fig. 3). From week 3 to week 10 of the precipitation tests, pH ranged from 5.79 to 5.84.

In test solution P–1A, an increase in pH over the first 24 hours of reaction was followed by a decrease in pH at week 1 of the test (Fig. 3). The pH of test solution P-1A increased from week 2 to 4 and then remained relatively constant over the remainder of the test (pH range of 5.95 to 5.96 from week 5 to 10). The increase in pH over the first 24 hours suggests that test solution P–1A may not have been in equilibrium with atmospheric PCO_2 prior to adding the synthesized uranophane. Because the pH increased over the first 24 hours, the pH of test solution P–1A was consistently higher than in the other precipitation test solutions.

The decrease in test solution pHs in the early parts of the experiments (e.g., from 24 hours to week 5 of the dissolution tests and from 24 hours to week 2 of the precipitation tests) was independent of initial dissolved uranyl concentrations, suggesting a surface phenomenon such as hydroxide sorption on a positively charged uranophane surface or Ca^{2+} exchange with H^{+}.

4.1.2. Ca

Rapid dissolution of uranophane is indicated by the initial increase in the Ca content of the uranophane dissolution test solutions (Fig. 2). Similarly, rapid precipitation of a Ca-bearing phase is indicated by the initial decrease in the Ca content of the uranophane precipitation test solutions (Fig. 3). After initial increase and decrease in Ca

content of the test solutions, a general trend of increasing Ca content over the duration of both the dissolution and precipitation test solutions is observed. The trend of increasing Ca content results from the effects of evaporation. Measurement of test solution masses before and after sampling indicates that, over a 1-week sampling interval, dissolution test solutions lost on average 0.65 ± 0.15 g [0.023 ± 0.005 oz] of mass, and precipitation tests solutions lost on average 0.34 ± 0.12 g [0.012 ± 0.004 oz] of mass by evaporation. The effects of evaporation on Ca contents are greater in the latter stages of the tests as the mass of the test solutions progressively decreases due to sampling (i.e., weekly removal of 10 g [0.35 oz] of solution for pH and cation analysis).

Mass transfer of Ca was characterized by net release of Ca in the dissolution experiments and net precipitation of Ca in the precipitation experiments (Figs. 4 and 5). Initial rapid Ca release in the dissolution experiments and initial rapid precipitation of Ca in the precipitation experiments was followed, in general, by erratic Ca release in the early parts of both the dissolution and precipitation experiments. The erratic Ca release suggests that evaporation is important. Evaporation could push solutions to slightly supersaturated conditions, resulting in precipitation of uranophane and/or another Ca-bearing phase. In the latter stages of the tests, Ca release tended to be relatively steady (i.e., moles of Ca released varied over a narrower range), suggesting that test solutions and solids were near equilibrium.

4.1.3. Si

Precipitation of a Si-bearing phase or phases is strongly suggested by the general trend of decreasing Si content in the early stages (e.g., from 24 hours to week 4 or 5) of both the dissolution and precipitation tests (Figs. 2 and 3). The general trend of increasing Si content in the latter stages of the dissolution tests (i.e., week 5 to week 10; Fig. 2) is again attributed to the effects of evaporation. On the other hand, the relatively

constant Si content of solutions in the latter stages of the precipitation tests (i.e., week 3 to week 10; Fig. 3) suggests a balance between evaporation and Si precipitation. Note from the previous section that dissolution test solutions lost on average 0.65 ± 0.15 g [0.023 ± 0.005 oz] of mass weekly, whereas precipitation tests solutions lost on average 0.34 ± 0.12 g [0.012 ± 0.004 oz] of mass weekly—about a two-fold difference. In the dissolution tests, the effects of evaporation could outweigh the effects of Si precipitation, resulting in the observed overall trend of increasing Si content in the latter stages of the tests.

Mass transfer of Si was characterized by net precipitation of Si in both the dissolution and precipitation experiments (Figs. 4 and 5). Initial precipitation of Si was followed by a general trend of continued Si precipitation over the first part of the dissolution and precipitation tests. Like Ca, evaporative effects could push solutions to slightly supersaturated conditions, resulting in precipitation of a Si-bearing phase or phases. Si release tended to be relatively steady (i.e., moles of Si released varied over a narrower ranges) in the latter stages of the dissolution and precipitation tests, suggesting that test solutions and solids were near equilibrium.

4.1.4. U

Despite differences in initial U concentrations of the dissolution and precipitation tests, measured U concentrations were remarkably similar; initial differences were largely eliminated after two weeks of reaction (Figs. 2 and 3). From week 3 to 10, U concentrations in the dissolution tests remained relatively constant, ranging from 1.13×10^{-7} to 3.82×10^{-7} M. In the precipitation tests, U concentrations from week 3 to 10 were observed to steadily increase over a limited concentration range. U concentrations in the precipitation tests ranged from 2.25×10^{-7} to 1.36×10^{-6} M from week 3 to 10. The

steady increase in the U contents of precipitation test solutions can again be attributed to the effects of evaporation.

Mass transfer of U was characterized by net release of U in the dissolution tests and net precipitation of U in the precipitation tests (Figs. 4 and 5). Initial U release in the dissolution tests and initial U precipitation in the precipitation tests was generally followed by U release up to week 4 in both the dissolution and precipitation tests. Uranium release up to week 4 following initial precipitation of U in the precipitation tests suggests dissolution of a U-bearing phase or phases. Note that chemical analyses of the synthesized uranophane indicated K contents of 1.5 to 2.0 ppm, suggesting the possible presence of residual boltwoodite. From week 5 onward, U release was generally steady in both the dissolution and precipitation tests, suggesting a balance between uranophane dissolution and precipitation.

Because total U concentrations tended toward values in limited ranges, uranyl (UO_2^{2+}) activities in the dissolution and precipitation tests, as determined using EQ3NR, also tended toward values in a limited range. From week 3 to 10, log[UO_2^{2+}] ranged from -8.09 to -8.39 in the precipitation tests and from -7.46 to -8.32 in the precipitation tests. The near-neutral pH of the test solutions also helped limit the range of UO_2^{2+} activities by limiting the formation of the uranyl-hydroxide and uranyl-hydroxy-carbonate species [e.g., $UO_2(OH)_3^-$ and $(UO_2)_2CO_3(OH)_3^-$] that would form at higher pH.

4.2 Evaluation of Soddyite Precipitation

Net precipitation of Si in relation to net release of Ca and U in dissolution test solutions suggests precipitation of a secondary Si-bearing phase or phases. Likewise, after initial precipitation of Ca, Si, and U in the precipitation tests, continued precipitation of Si in contrast to release of Ca and U from week 1 to week 4 (Fig. 5) also suggests

precipitation of a secondary Si-bearing phase or phases. Calculation of mineral saturation states in the test solutions using the EQ3NR geochemical code indicates supersaturation with the uranyl silicate soddyite [$(UO_2)_2SiO_4 \cdot 2H_2O$] and saturation with amorphous silica.

In laboratory-scale corrosion tests of synthetic UO_2 and spent UO_2 fuel under conditions designed to simulate a potential Yucca Mountain repository, soddyite has been identified in the paragenetic sequence of alteration phases (Finch et al., 1999; Wronkiewicz et al., 1992, 1996). Soddyite was observed to succeed the formation of uranyl oxide hydrates and precede the formation of alkaline earth and alkali uranyl silicates, such as uranophane and boltwoodite. Soddyite has been observed in a similar progression of secondary uranyl phases formed by weathering of uraninite at the Nopal I uranium deposit in Mexico (Pearcy et al., 1994).

To evaluate the potential for soddyite precipitation in the uranophane solubility tests, dissolution and precipitation test solution chemistries were evaluated with respect to the solubility limit of soddyite. Mass transfer results indicate that release of Si and U was relatively steady in the latter stages of the dissolution and precipitation tests. The log activities of $UO_2^{2+}/(H^+)^2$ versus SiO_2(aq) in test solutions for the last four sampling intervals (i.e., samples taken at 7 to 10 weeks) with respect to the solubility limit of soddyite are plotted in Fig. 7.

Fig. 7 illustrates that the activities in the dissolution test solutions tended toward a limit corresponding to undersaturation with soddyite. The activities of precipitation test solutions P–1A and P–1B, which had initial Si concentrations of ~10^{-3} M, also tended toward a limit corresponding to undersaturation with soddyite. However, when compared to the dissolution test solutions, the activities of test solutions P–1A and P–1B more closely approached the soddyite solubility limits. The activities of precipitation test solutions P–2A and P–2B, which had initial Si concentrations of ~2.0×10^{-3} M, tended

toward a limit corresponding to supersaturation with soddyite when compared to the soddyite limit of Nguyen et al. (1992) and toward a limit corresponding to equilibrium or slight supersaturation with soddyite when compared to the soddyite limit of Giammer and Hering (2002).

4.3 Extraction of Log K for Uranophane Dissolution

General trends in the mass transfer data indicate that elemental release of all three uranophane components (i.e., Ca, Si, and U) were relatively steady, suggesting near equilibrium with uranophane in the latter stages of the tests (e.g., at 7 to 10 weeks). For the last four sampling intervals, the range of log Qs for uranophane in the dissolution tests was 10.57 to 11.06, and the range of log Qs for uranophane in the precipitation tests was 11.30 to 12.22. The log Q midpoint separating these two ranges is 11.18, and this value was taken as the best approximation for the uranophane equilibrium constant (log K). The standard deviation in the log Qs for the combined dissolution and precipitation tests was calculated to be 0.54.

Using a log K for uranophane dissolution of 11.18 ± 0.54 and standard state Gibbs free energy data from Guillaumont et al. (2003) for components of the uranophane reaction in Eq. 3, the standard Gibbs free energy of formation for uranophane and the uranophane dissolution reaction can be determined. These values are -6195.2 ± 3.1 kJ mol^{-1} [$-1.4807 \times 10^6 \pm 740.9$ cal mol^{-1}] for uranophane and -63.8 ± 3.1 kJ mol^{-1} [$-1.5248 \times 10^4 \pm 740.9$ cal mol^{-1}] for the uranophane dissolution reaction.

4.4 Comparison to Other Studies

Efforts to measure uranophane solubility in previous studies have proven to be difficult and have produced inconsistent results. Nguyen et al. (1992) conducted a dissolution experiment using synthesized uranophane and reported a log K of 9.4 ± 0.5

for the reaction shown in Eq. 3. This value was derived from a single experimental solution from an experiment conducted at low pH (3.50 ± 0.05) under an Ar atmosphere. Murphy and Pabalan (1995) concluded that the uranophane solubility data reported by Nguyen et al. (1992) are unreliable due to the non-nominal stoichiometric solid phase composition of the synthesized uranophane and incongruent elemental release in the dissolution experiments. Measured concentrations of U and Si in the synthesized uranophane agreed well with the nominal stoichiometric values for uranophane, but Ca was lower than the stoichiometric value. Reported concentrations of Si, U, and Ca in the experimental solutions suggest incongruent elemental release, which probably resulted from secondary phase precipitation.

Perez et al. (2000) reported log K values that ranged from 10.75 to 12.94 for uranophane from dissolution experiments with an average log K value of 11.7 ± 0.6, for the reaction

$$Ca(UO_2)_2Si_2O_7 \cdot 6H_2O + 6HCO_3^- \leftrightarrow Ca^{2+} + 2UO_2(CO_3)_3^{4-} + 2H_4SiO_4 + 5H_2O. \quad (5)$$

The uranophane dissolution experiments were carried out in bicarbonate solutions in contact with air. Equilibrium pH in the test solutions ranged from 8.65 to 9.37. Uranium speciation calculated by Perez et al. (2000) showed that, at the total bicarbonate concentrations of the test solutions, the $UO_2(CO_3)_3^{4-}$ complex is the dominant aqueous species. Therefore, the uranophane dissolution reaction shown in Eq. 5 was invoked for the log K calculation, and all U was attributed to the $UO_2(CO_3)_3^{4-}$ species. The uranophane used in the experiments was synthesized following the procedure of Nguyen et al. (1992), and chemical analyses again showed a deficiency in Ca. Data trends in two of the experimental test solutions also indicated the possibility of formation of a secondary solid phase. Using the log K value of 11.7 ± 0.6, Perez et al. (2000)

estimated a free energy of formation for uranophane of -6192.3 ± 3.4 kJ mol^{-1} [-1.4799 × 10^6 ± 812.6 cal mol^{-1}]. Despite the non-nominal stoichiometry of the synthesized uranophane and the likelihood of incongruent elemental release in the dissolution experiments, the calculated free energy of formation for uranophane of -6192.3 ± 3.4 kJ mol^{-1} [1.4799 × 10^6 ± 812.6 cal mol^{-1}] reported by Perez et al. (2000) is in close agreement with the measured free energy of formation for uranophane of -6195.2 ± 3.1 kJ mol^{-1} [-1.4807 × 10^6 ± 740.9 cal mol^{-1}] in this study.

Chen et al. (1999) developed a semiempirical method for estimating free energies and enthalpies of formation for uranyl phases by summing contributions of the component polyhedral units of the minerals. According to this model, when silica concentrations exceed ~10^{-4} M, uranyl silicate phases such as uranophane and soddyite are predicted to be the thermodynamically favored solids. Based on the method, Chen et al. (1999) estimated a free energy of formation of uranophane of -6189.2 kJ mol^{-1} [-1.4793 × 10^6 cal mol^{-1}].

A logarithmic activity diagram of $UO_2^{2+}/(H^+)^2$ versus SiO_2(aq) versus $Ca^{2+}/(H^+)^2$ illustrating the position of test solution chemistries for the last four sampling intervals from the dissolution and precipitation tests, is plotted in Fig. 8. The solubility limit of uranophane based on the results of this study (i.e., calculated using a log K of 11.18) and the solubility limit of uranophane estimated by Chen et al. (1999) are also plotted on the activity diagram. The estimated solubility limit of uranophane was calculated using an equilibrium constant (log K) for uranophane dissolution of 12.30, which was derived from Eq. 3 and the estimated standard state free energy of formation of uranophane {-6189.2 kJ/mol^{-1} [-1.4793 × 10^6 cal mol^{-1}]} reported by Chen et al. (1999) and free energy data for other reactants from Guillaumont et al. (2003). When compared to the prediction of Chen et al. (1999), dissolution test solutions and precipitation test solutions P–1A and P–1B tend toward a limit corresponding to undersaturation with respect to

uranophane. On the other hand, precipitation test solutions P–2A and P–2B, which had twice the SiO_2(aq) activity and showed evidence of possible soddyite precipitation, tend toward a limit approaching equilibrium with respect to the Chen et al. (1999) estimated solubility limit of uranophane.

4.5 Significance to SNF Corrosion

Uranyl minerals are the solubility-limiting phases of uranium during the oxidative alteration of SNF. If containers were breached at a potential Yucca Mountain repository and water contacted the SNF, the dissolved concentration of U and the potential secondary phase immobilization of actinides and fission products would depend largely on the structures and stabilities of the secondary phases formed. Uranophane has been shown to be the end product of the paragenetic sequence of uranyl minerals that are produced by corrosion of spent UO_2 fuel and weathering of uraninite ($UO_{2+x,}$ an analog for SNF) in U ore deposits hosted by siliceous volcanic rocks (Finch et al., 1999; Pearcy et al., 1994; Wronkiewicz et al., 1992, 1996). Dating of uranophane from the Nopal I U deposit (Pickett and Leslie, 2005; Pickett and Murphy, 1997), a natural analog to a potential Yucca Mountain geologic repository, suggests that uranophane is chemically stable in the natural environment on a geologic time scale (e.g., 10^4 to 10^6 years) comparable to the period of regulatory concern for a potential Yucca Mountain repository. Thus, a reasonable predictive model for assessing the performance of a potential Yucca Mountain repository should include an examination of uranophane and its potential to influence the dissolved concentration and mobility of spent fuel waste species.

Retention of radionuclides by secondary uranium phases formed during spent fuel alteration has been the subject of much speculation and experimentation (Murphy and Codell, 1999; Buck et al., 1998; Burns, 1999; Burns and Hill, 2000; Burns et al., 1997;

Finch et al., 1999, 2002). Several uranyl solids have been shown experimentally to incorporate low valance cations such as cesium and strontium into their structures (Burns, 1999; Burns and Hill, 2000). However, results of such studies with Np, a long-lived radionuclide that may affect the long-term safety of the potential Yucca Mountain repository, are ambiguous. Np retention by dehydrated schoepite, $UO_3 \cdot 0.8H_2O$, was reported by Buck et al. (1998) during spent fuel corrosion studies. TEM-EELS analysis indicated that Np was associated with the dehydrated schoepite at approximately 550 ppm concentration. However, a reevaluation of Np in the dehydrated schoepite derived in the spent fuel corrosion studies by Fortner et al. (2003, 2004) indicated that identification of Np in the EELS analysis was a spurious artifact of the U spectrum. Fortner et al. (2003, 2004) used X-ray absorption analysis to demonstrate little or no Np incorporation in dehydrated schoepite from the spent fuel corrosion studies. Other recent studies also show that synthetic schoepite and dehydrated schoepite do not incorporate Np (Burns et al., 2004).

Bond-valence calculations indicate that the neptunyl (NpO_2^+) cation can be accommodated in the uranophane structure by substitution for the uranyl (UO_2^{2+}) cation and incorporation of other charge-balancing cations (Burns et al., 1997). The incorporation of other charge-balancing cations is necessary because substitution of NpO_2^+ for UO_2^{2+} alone will result in a charge deficit. Incorporation of Np by uranyl silicates, including uranophane, was not observed during spent fuel corrosion studies conducted by Finch et al. (1999) and was attributed to the lack of charge-balancing cations in the experiments. Recently, Burns et al. (2004) and Douglas et al. (2005) have investigated Np incorporation into synthetically prepared uranyl phases. In both these studies, charge-balancing cations (e.g., Na) were included in the syntheses. Burns et al. (2004) reported the possible incorporation of Np into uranophane and Na-compregnacite, $Na_2[(UO_2)_3O_2(OH)_3]_2(H_2O_7)$, at levels in proportion to the Np-

concentration level of the solutions from which they formed. In the investigations of Douglas et al. (2005), uranophane and Na-boltwoodite, $Na[(UO_2)(SiO_3OH)] \cdot 1.5H_2O$ were also found to contain levels of Np in proportion to the concentration level of the solutions from which they were precipitated. From the standpoint of performance at a potential Yucca Mountain repository, the incorporation of Np into synthetic uranophane in the presence of charge-balancing cations may provide a long-term mechanism for Np retention.

5. CONCLUSIONS

Laboratory experiments were conducted to examine the thermodynamics of dissolution and growth of uranophane in Ca- and Si-rich test solutions at low temperatures {20.5 ± 2.0 °C [68.9 ± 3.6 °F) and near-neutral pH (~6.0). Initial U concentrations of experimental solutions were selected so that reaction of uranophane would approach equilibrium from both undersaturation and supersaturation. Experimental solutions were reacted with synthetic uranophane and analyzed periodically over a 10-week period. Sampling schemes were chosen to track the concentration and mass transfer of uranophane components (i.e., Ca, Si, and U) as a function of time and solution pH. The effects of sampling and evaporation on Ca, Si, and U solution concentrations over the duration of the tests were accounted for in the cumulative mass transfer calculations by measuring experimental solution masses before and after each sampling interval.

Mass transfer results indicated precipitation of a secondary Si-bearing phase or phases (e.g., soddyite or amorphous silica) in both the dissolution and precipitation tests. An evaluation of test solution chemistries with respect to experimentally and theoretically derived solubility limits for soddyite indicated that dissolution test solutions and precipitation test solutions P–1A and P–1B were undersaturated with soddyite. All

of these test solutions had initial Si concentrations of ~10^{-3} M. On the other hand, the position of precipitation test solutions P–2A and P–2B with respect to the solubility limits of soddyite indicated supersaturation or equilibrium with soddyite. Test solutions P-2A and P-2B had higher initial Si concentration of ~2 × 10^{-3} M.

Trends in the pH and mass transfer data indicated that pH and elemental release of all three uranophane components (i.e., Ca, Si, and U) were relatively steady in the latter stages of the tests (e.g., at 7 to 10 weeks), suggesting that test solutions were in near equilibrium with uranophane. Based on test solution chemistries in the last four sampling intervals of the dissolution and precipitation tests, a log K of 11.18 for uranophane dissolution was approximated. This value was derived by taking the midpoint separating the ranges of calculated log Qs for the dissolution and precipitation tests. The standard deviation in the log K for uranophane was estimated to be 0.54 and was derived from calculated log Qs for the combined dissolution and precipitation tests.

Using the log K for uranophane dissolution of 11.18 ± 0.54, a Gibbs free energy of formation for uranophane of -6195.2 ± 3.1 kJ mol^{-1} [-1.4807 × 10^{6} ± 740.9 cal mol^{-1}] was calculated. Precipitation of uranophane in this study, based on mass transfer data, is consistent with the widespread occurrence of uranophane in oxidizing low temperature U deposits (Pearcy et al., 1994). Determination of a reversed solubility for uranophane (i.e., an approach to uranophase equilibrium from supersaturated conditions) places an additional constraint on the thermodynamic data needed to predict the stability of uranophane, especially under conditions (e.g., low temperature and near-neutral pH) that are expected to exist over the period of regulatory concern at a potential Yucca Mountain repository. More importantly, the results of this study provide useful thermodynamic data for future work on Np incorporation in uranophane to assess the Np solubility limitduring SNF degradation at the potential Yucca Mountain repository.

Acknowledgments—The author acknowledges and thanks W.M. Murphy, who contributed substantially to the conceptual design and interpretation of the results of this experimental study. D. Pickett, G. Wittmeyer, and two anonymous reviewers provided constructive reviews. Assistance from N. Naukam in preparing the document is gratefully acknowledged.

This paper was prepared to describe work performed by the Center for Nuclear Waste Regulatory Analyses (CNWRA) for the U.S. Nuclear Regulatory Commission (NRC) under Contract No. NRC–02–02–012. The activities reported here were performed on behalf of the NRC Office of Nuclear Materials Safety and Safeguards, Division of High-Level Waste Repository Safety. This paper is an independent product of CNWRA and does not necessarily reflect the view or regulatory position of NRC.

References

Buck E. C., Finch R. J., Finn P. A., and Bates J. K. (1998) Retention of Np in uranyl alteration phases formed during spent fuel corrosion. In *Scientific Basis for Nuclear Waste Management XXI Materials Research Society Symposium Proceedings Vol. 506* (eds. I. G. McKinley and C. McCombie). Materials Research Society, Warrendale, PA, p 83.

Burns P. C. (1999) Cs boltwoodite obtained by ion exchange of single crystals: Implications for radionuclide release in a nuclear repository. *J. Nucl. Mater*. **265**, 218.

Burns P. C., Ewing R. C., and Miller M. L. (1997) Incorporation mechanisms of actinide elements into the structures of U^{6+} phases formed during the oxidation of spent nuclear fuel. *J. Nucl. Mater.* **245**, 1-9.

Burns P. C., Deely K. M., and Skanthakumar S. (2004) Neptunium incorporation into uranyl compounds that form as alteration products of spent nuclear fuel: Implications for geologic repository performance. *Radiochim. Acta* **92**, 151-159.

Burns P. C. and Hill F. C. (2000) Implications of the synthesis and structure of the Sr analogue of curite. *Can. Mineral*. **38**, 175.

Chen F., Ewing R. C., and Clark S. B. (1999) The Gibbs free energy and enthalpies of formation of U^{6+} phases: An empirical method of prediction. *American Mineralogist* **84**, 650-664.

Douglas M., Clark S. B., Friese J. I., Arey B. W., Buck E. C., Hanson B. D., Utsunomiya S., and Ewing R. C. (2005) Microscale characterization of uranium (VI) silicate solids and associated neptunium (V). *Radiochim. Acta* **93**, 265-272.

Finch R. J. and Ewing R. C. (1992) The corrosion of uraninite under oxidizing conditions. *J. Nucl. Mater.* **190**, 133-156.

Finch R. J. and Murakami T. (1999) Systematics and paragenesis of uranium minerals. In *Uranium: Mineralogy, Geochemistry and the Environment* (eds. P. C. Burns and R. Finch), *Rev. Mineral*. **38**, 91-180. Mineralogical Society of America, Washington, DC.

Finch R. J., Suksi J., Rasilainen K., and Ewing R. C. (1996) U-series ages of secondary uranium minerals with applications to the long-term evolution of spent nuclear fuel. In *Scientific Basis for Nuclear Waste Management XIX Materials Research Society Symposium Proceedings Vol. 412* (eds. W. M. Murphy and D. A. Knecht). Materials Research Society, Warrendale, PA, pp. 823-830.

Finch R. J., Buck E. C., Finn P. A., and Bates J. K. (1999) Oxidative corrosion of spent UO_2 fuel in vapor and dripping groundwater at 90 °C. In *Scientific Basis for Nuclear Waste Management XIX Materials Research Society Symposium Proceedings Vol. 556* (eds. D. J. Wronkiewicz and J. H. Lee). Materials Research Society, Warrendale, PA, pp. 431-438.

Finch R. J., Fortner J. A., Buck E. C., and Wolf S. F. (2002) Neptunium incorporation into uranium (VI) compounds formed during aqueous corrosion of neptunium-bearing uranium oxides. In *Scientific Basis for Nuclear Waste Management XXV Materials Research Society Symposium Proceedings Vol. 713* (eds. B. P. McGrail and G. A. Cragnolino). Materials Research Society, Warrendale, PA, p. 647.

Finn P. A., Finch R. J., Buck E. C., and Bates J. K. (1998) Corrosion mechanisms of spent fuel under oxidizing conditions. In *Scientific Basis for Nuclear Waste Management XXI Materials Research Society Symposium Proceedings Vol. 506* (eds. I. G. McKinley and C. McCombie). Materials Research Society, Warrendale, PA, pp. 123-131.

Fortner J. A., Finch R. J., Kropf A. J., and Cunnane J. C. (2003) Reevaluating neptunium in uranyl phases derived from corroded spent fuel. Proceedings of the 2003 International High-Level Radioactive Waste Management Conference, Las Vegas, NV, March 30-April 2 (2003), American Nuclear Society Proceedings.

Fortner J. A., Finch R. J., Kropf A. J., and Cunnane J. C. (2004) Re-evaluating neptunium in uranyl phases derived from corroded spent fuel. *J. Nuclear Technology* **148**, 174-180.

Giammer D. E. and Hering J. G. (2002) Equilibrium and kinetic aspects of soddyite dissolution and secondary phase precipitation in aqueous suspension. *Geochim. Cosmochim. Acta* **66**, No. 18, 3235-3245.

Guillaumont R., Fanghanel T., Fuger J., Grenthe I., Neck V., Palmer D. A., and Rand M. H. (2003) Update on the chemical thermodynamics of uranium, neptunium, plutonium, americium and technetium. *Chemical Thermodynamics Series 5* (eds. F. J. Mompean, M. Illemassene, C. Domenech-Orti, and K. Ben-Said). Elsevier, 970 p.

ICDD: Powder Diffraction File PDF-2 Database Sets 1-43 (1993) International Centre for Diffraction Data, Swarthmore, PA.

ICDD: Mineral Powder Diffraction File Data Book (1986) International Centre for Diffraction Data, Swarthmore, PA.

Johnson L. H. and Shoesmith D. W. (1988) Spent Fuel. In *Radioactive Waste Forms for the Future.* (eds. W. Lutze and R. C. Ewing). Elsevier, pp. 635-698.

Murphy W. M. and Codell R. B. (1999) Alternate source term models for Yucca Mountain performance assessment bored or natural analog data and secondary mineral solubility. In *Scientific Basis for Nuclear Waste Management XXII* (eds. D. J. Wronkiewicz and J. Lee). Material Research Society, Warrendale, PA. pp. 551-558.

Murphy W. M. and Pabalan R. T. (1995) Review of Empirical Thermodynamics Data for Uranyl Silicate Minerals and Experimental Plan. Center for Nuclear Waste Regulatory Analyses, San Antonio, Texas, CNWRA 95-014, p. 43.

Nguyen S. N., Silva R. J., Weed H. C., and Andrews, Jr., J. E. (1992) Standard Gibbs free energy of formation at the temperature 303.15K of four uranyl silicates: Soddyite, uranophane, sodium boltwoodite, and sodium weeksite. *J. Chem. Thermodynam.* **24**, 359-376.

Oversby V. M. (1994) Nuclear Waste Materials. In *Materials Science and Technology, A Comprehensive Treatment, Nuclear Materials 10B* (ed. B. R. T. Frost). VCH: Weinheim, Germany, pp. 392-442.

Pearcy E. C., Prikryl J. D., Murphy W. M., and Leslie B. W. (1994) Alteration of Uraninite from the Nopal I Deposit, Peña Blanca District, Chihuahua, Mexico, Compared to Degradation of Spent Nuclear Fuel in the Proposed U.S. High-Level Nuclear Waste Repository at Yucca Mountain, Nevada. *Appl. Geochem.* **9**, 713-732.

Perez I., Casas I., Martin M., and Bruno J. (2000) The Thermodynamics and Kinetics of Uranophane Dissolution in Bicarbonate Test Solutions. *Geochim. Cosmochim. Acta* **64**, 4, 603-608.

Pickett D. A. and Leslie B. W. (2005) Mobilization of Uranium from the Nopal I analog and implications for nuclear waste repository performance. *Annual Meeting Geological Society of America*. Geological Society of America Abstracts with Programs, Vol. 37, No. 7, p. 268.

Pickett D. A. and Murphy W. M. (1997) Isotopic constraints on radionuclide transport at Pena Blanca. *Seventh EC Natural Analogue Working Group Meeting Proceedings, EUR 17851 EN* (eds. H. Von Maravic and J. Smellie). Nuclear Science and Technology Series. Stein am Rhein, Switzerland: Luxembourg: European Communities. pp. 113-122.

Prikryl J. D. and Murphy W. M. (2004) The dissolution of uranophane in CcCl2-SiO2(aq) test solutions. In *Scientific Basis for Nuclear Waste Management XXVIII Materials Research Society Symposiun Proceedings* (eds. J. M. Hanchar, S. Stroes-Gascoyne, and L. Browning). Materials Research Society, Warrendale, PA. pp. 189-194.

Vochten R., Blanton N., Peeters O., Van Springel K., and Van Haverbeke L. (1997) A new method of synthesis of boltwoodite and of formation of sodium boltwoodite, uranophane, sklodowskite and kasolite from boltwoodite. *Canadian Mineralogist* **35**, 735-741.

Wolery T. (1992) EQ3/6, A software package for geochemical modeling of aqueous systems. UCRL-MA-110662 PT1, Lawrence Livermore National Laboratory, Livermore, CA.

Wronkiewicz D. J., Bates J. K., Gerding T. J., Veleckis E., and Tani B. S. (1992) Uranium Release and Secondary Phase Formation During Unsaturated Testing of UO_2 at 90 ºC. *J. Nucl. Mater.* **190**, 107-127.

Wronkiewicz D. J., Bates J. K., Wolf S. F., and Buck E. C. (1996) Ten-year results from unsaturated drip tests with UO2 at 90 °C: Implications for the corrosion of spent nuclear fuel. *J. Nucl. Mater.* **238**, 78.

Table 1. Measured initial U, Ca, and Si concentrations and pH of the uranophane solubility test solutions. Intended pHs and Ca, Si, and U concentrations were pH ~6.0, Ca ~10^{-2} M, Si ~10^{-3} M, and U = 0.0 or ~10^{-7} M for the dissolution tests and pH ~6.0, Ca ~10^{-2} M, Si ~10^{-3} or ~2×10^{-3} M, and U ~10^{-6} or ~2×10^{-6} M for the precipitation tests.

Test Label	U (M)	Ca (M)	Si (M)	pH
Dissolution Tests				
D–0A	0	9.63×10^{-3}	1.19×10^{-3}	6.05
D–0B	0	9.64×10^{-3}	1.22×10^{-3}	6.05
D–7A	9.66×10^{-8}	9.69×10^{-3}	1.22×10^{-3}	5.98
D–7B	9.66×10^{-8}	9.69×10^{-3}	1.20×10^{-3}	5.98
Precipitation Tests				
P–1A	1.24×10^{-6}	9.04×10^{-3}	1.16×10^{-3}	6.02
P–1B	2.41×10^{-6}	9.07×10^{-3}	1.16×10^{-3}	5.99
P–2A	9.08×10^{-7}	9.08×10^{-3}	2.32×10^{-3}	5.95
P–2B	1.98×10^{-6}	9.04×10^{-3}	2.26×10^{-3}	6.00

Table 2. The ranges of the logarithms of activities of Ca^{2+}, $SiO_2(aq)$, UO_2^{2+}, and H^+ and calculated ranges of the logarithms of reaction quotients (log Q) for uranophane dissolution in the uranophane dissolution and precipitation test solutions.

Test Label	log[Ca^{2+}]	log[SiO_2(aq)]	log[UO_2^{2+}]	log[H^+]	log Q
Dissolution Tests					
D–0A	-2.28 to -2.25	-2.94 to –2.92	-8.70 to -8.12	-6.03 to -5.88	10.63 to 11.00
D–0B	-2.27 to -2.25	-2.94 to –2.91	-8.74 to -8.16	-6.06 to -5.89	10.61 to 11.03
D–7A	-2.27 to -2.25	-2.93 to –2.91	-8.47 to -8.19	-6.04 to -5.86	10.54 to 11.18
D–7B	-2.27 to -2.25	-2.93 to -2.91	-8.48 to -8.07	-6.02 to -5.84	10.75 to 11.14
Precipitation Tests					
P–1A	-2.30 to -2.29	-2.96 to -2.95	-8.88 to -8.00	-6.07 to -5.91	10.20 to 11.48
P–1B	-2.30 to -2.29	-2.95 to -2.94	-8.58 to -7.70	-5.97 to -5.82	10.47 to 11.40
P–2A	-2.30 to -2.29	-2.64 to -2.63	-8.61 to -7.50	-5.95 to -5.78	10.90 to 12.18
P–2B	-2.30 to -2.29	-2.65 to -2.64	-8.36 to -7.47	-5.94 to -5.79	11.02 to 12.22

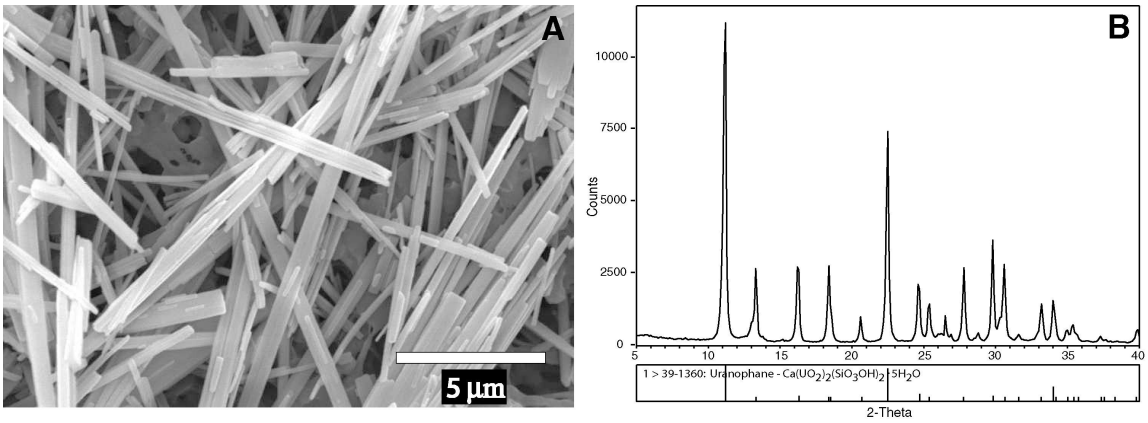

Fig. 1. (A) Scanning electron photomicrograph of uranophane synthesized for use in the solubility experiments. (B) X-ray diffraction (XRD) pattern of the synthesized uranophane compared to a reference pattern taken from the International Centre for Diffraction Data database (1993).

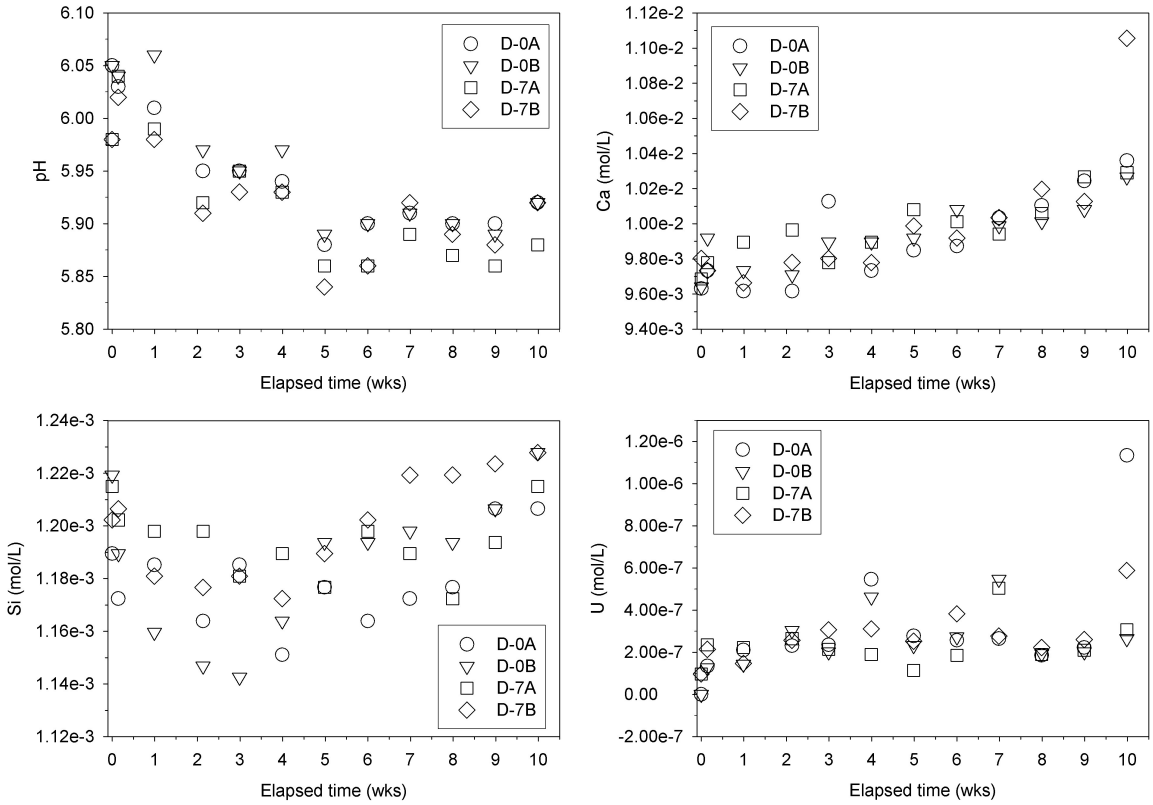

Fig. 2. The pH and concentrations of Ca, Si, and U in uranophane dissolution test solutions plotted as a function of time.

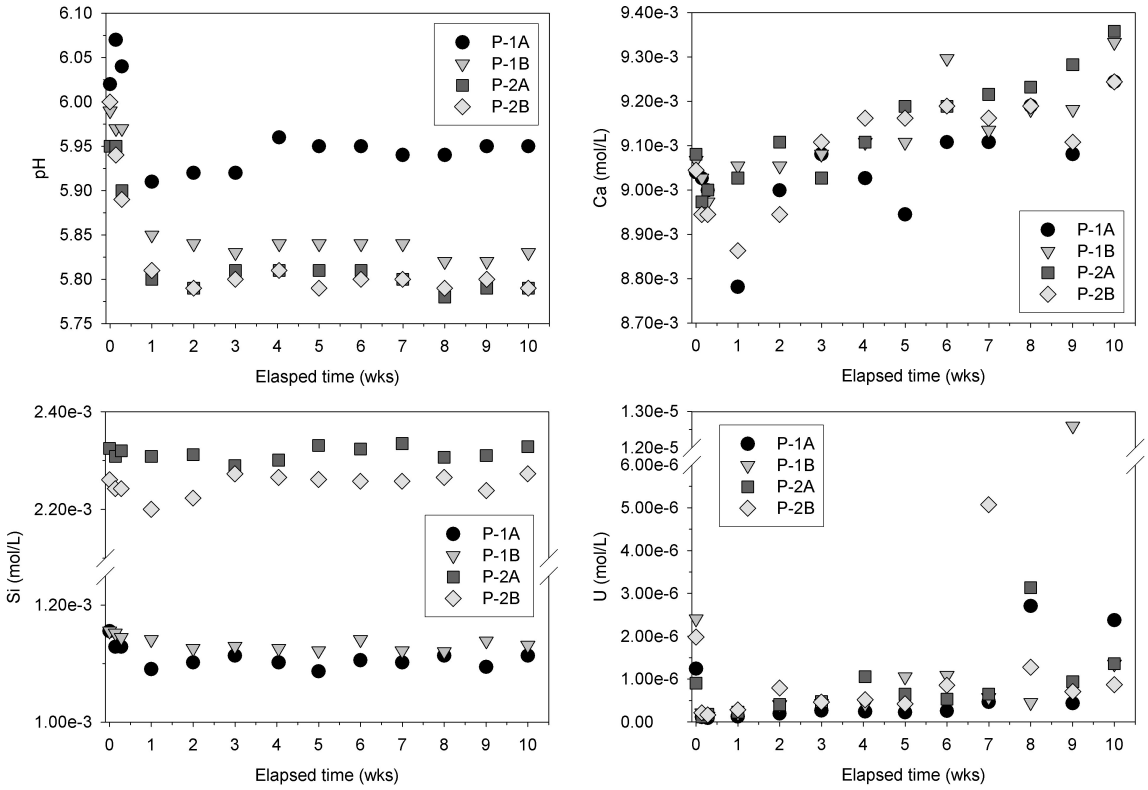

Fig. 3. The pH and concentrations of Ca, Si, and U in uranophane precipitation test solutions plotted as a function of time.

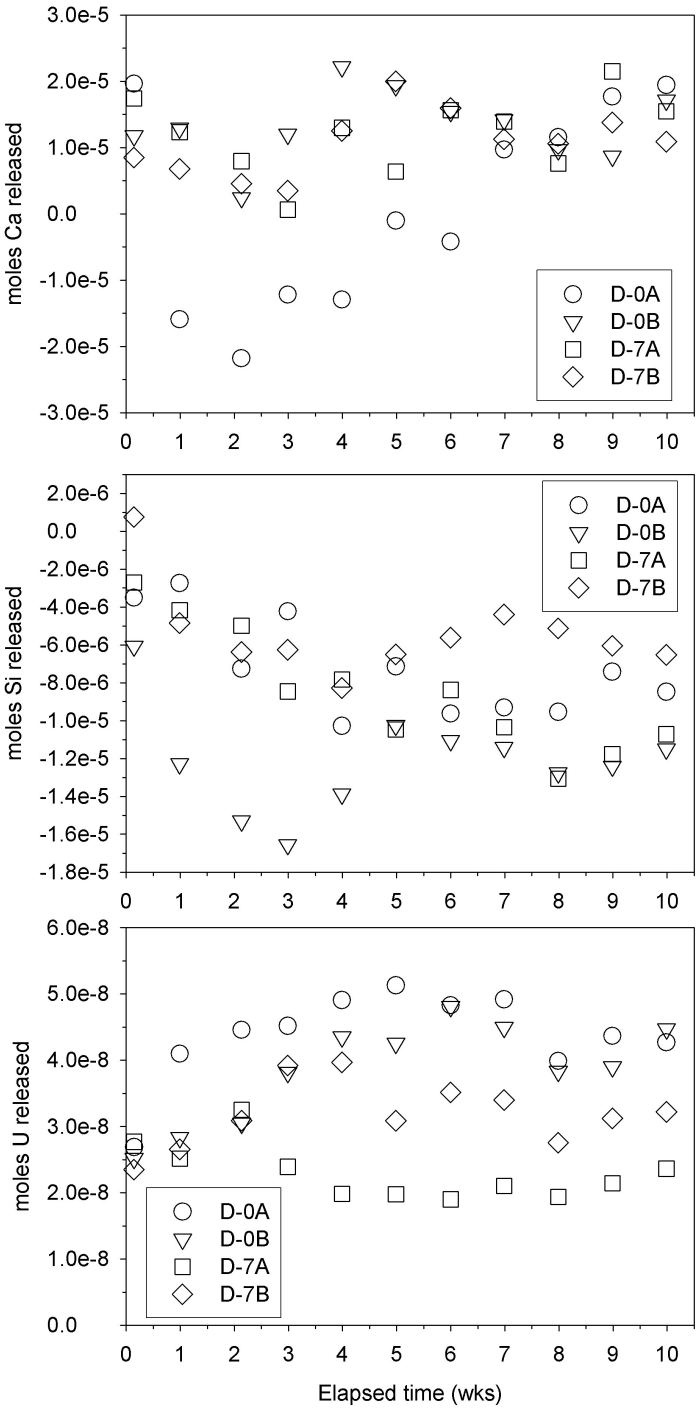

Fig. 4. Net moles of Ca, Si, and U released to solution in the uranophane dissolution tests plotted as a function of time.

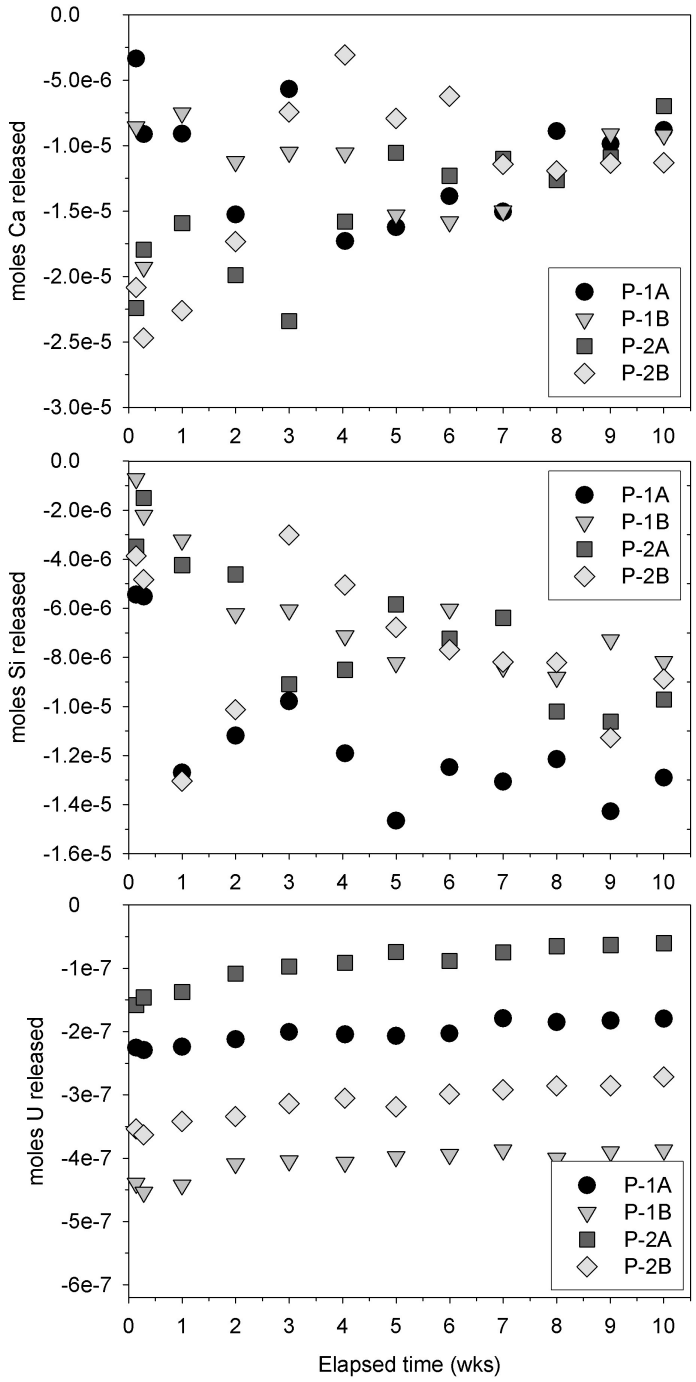

Fig. 5. Net moles of Ca, Si, and U released to solution in the uranophane precipitation tests plotted as a function of time.

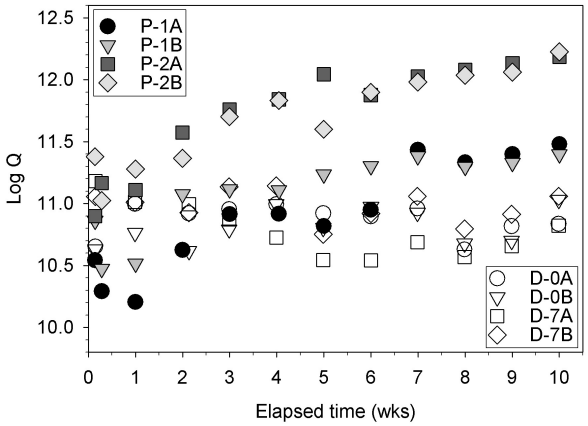

Fig. 6. Calculated log Qs for the uranophane dissolution in the dissolution and precipitation test solutions plotted as a function of time.

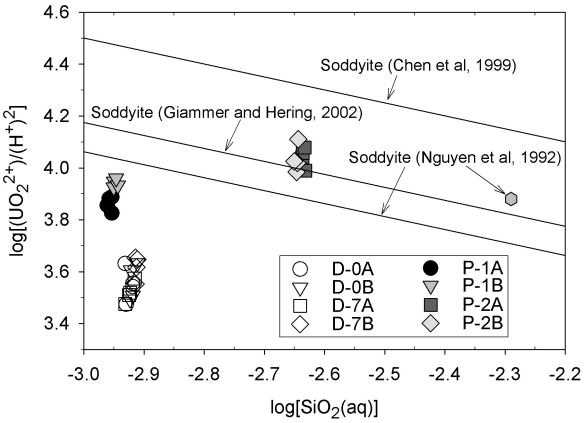

Fig. 7. Logarithmic activity diagram of $UO_2^{2+}/(H^+)^2$ versus SiO_2(aq) illustrating the position of the uranophane dissolution and precipitation test solutions with respect to the solubility limit of soddyite. Solubility limits for soddyite are based on experimental data of Nguyen et al. (1992), a recalculation of the experimental data of Nguyen et al. (1992) based on a new set of complexation reactions and ionic strength corrections (Giammer and Hering, 2002) and theoretical prediction (Chen et al., 1999). A single solution taken from a soddyite dissolution experiment conducted by Nguyen et al. (1992) is also plotted.

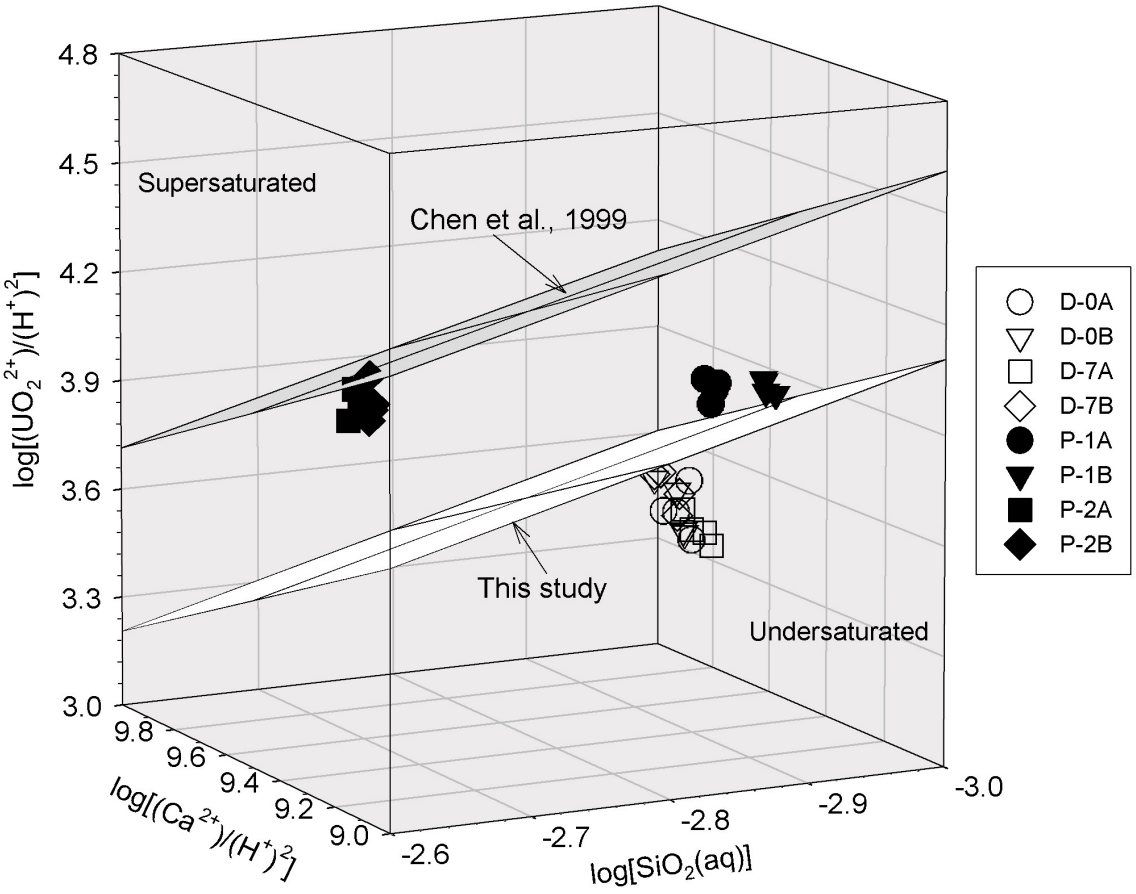

Fig. 8. Logarithmic activity diagram of $UO_2^{2+}/(H^+)^2$ versus $SiO_2(aq)$ versus $Ca^{2+}/(H^+)^{2,}$ illustrating the position of test solution chemistries for the last four sampling intervals with respect to the theoretical solubility limit of uranophane predicted by Chen et al. (1999) and the solubility limit of uranophane based on experimental data from this study.